Journal of Hydrology X 21 (2023) 100163

Contents lists available at ScienceDirect

Journal of Hydrology X

journal homepage: www.sciencedirect.com/journal/journal-of-hydrology-x

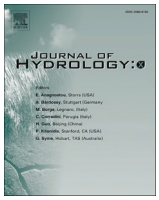

Research papers

The response of borehole water levels in an ophiolitic, peridotite aquifer to atmospheric, solid Earth, and ocean tides

R.A. Sohn [a,*], J.M. Matter [b]

[a] Woods Hole Oceanographic Institution, Woods Hole, MA 02543, USA
[b] Ocean and Earth Science, National Oceanography Centre Southampton, University of Southampton, United Kingdom

ARTICLE INFO

Keywords:
Borehole
Peridotite
Aquifer
Tides
Ophiolite

ABSTRACT

Peridotite aquifers are ubiquitous on Earth, but most are in the deep-sea, and thus difficult to access. Ophiolites provide a unique opportunity to study peridotite aquifers, and the Oman Drilling Project established a Multi-Borehole Observatory in a peridotite terrain of the Samail ophiolite. We use the water level response of two 400-m deep boreholes (BA1B, BA1D) to solid Earth, ocean, and atmospheric tides to investigate the hydromechanical structure of the aquifer. The two boreholes are offset by ~ 100 m but exhibit markedly different tidal responses, indicating a high degree of short-length-scale heterogeneity. Hole BA1B does not respond to tidal strain or barometric loading, consistent with the behavior of an unconfined aquifer. Hole BA1D responds to both tidal strain and barometric loading, indicating some degree of confinement. The response to applied strain, which includes a non-negligible ocean tidal loading component, is consistent with a partially confined, low conductivity aquifer. The response to barometric loading appears to be affected by the complex hydrological structure of the surficial zone and we were not able to fit the observations to within error. Aquifer conductivity estimates for Hole BA1D based on the response to tidal strain are within a factor of ~ 3 of pumping test estimates.

1. Introduction

Peridotite, the dominant rock of the Earth's upper mantle, is exposed across large areas of the Earth's outer surface, but peridotite aquifers are poorly understood because most exposures were formed, and are located, in the deep-sea. The interaction between water and peridotite is substantially different from that between water and most rocks - peridotite alteration is exothermic (Fyfe, 1974), increases the solid volume of the rock (Macdonald and Fyfe, 1985), dramatically changes the rock rheology (e.g., Reinen et al., 1994; Escartin et al., 2001), can sequester carbon (Kelemen et al., 2011), produces gases (e.g., H_2, CH_4, McCollom and Seewald, 2001), and generates reduced fluids that provide habitat for chemosynthetic organisms (e.g., Schrenk et al., 2013; Templeton et al., 2021). The unique qualities of the interaction between water and peridotite have stimulated a growing body of research regarding the geochemical and microbiological effects of peridotite alteration, but the hydrologic behavior of peridotite aquifers remains poorly understood. This knowledge gap is problematic because it inhibits, for example, our understanding of how subsurface biospheres are sustained, or how carbon might be safely sequestered, in these environments.

Peridotite aquifers are exposed on land in ophiolites, and these exposures provide an opportunity to study their hydrology without the logistical challenges of deep-sea environments. There have been relatively few hydrological studies of ophiolitic, peridotite aquifers, but Dewandel et al. (2005) synthesized catchment-scale, well-scale, and sample-scale analyses to develop a generalized hydrogeological model for hard rock aquifers in the Samail ophiolite (Oman). Large-scale fluid flow is accommodated by discrete fracture networks, and groundwater circulation is largely restricted to a ~ 50 m thick, surficial, fissured zone. Circulation at deeper depths is accommodated by hydraulically transmissive fractures, some of which are inherited from accretionary processes at mid-ocean ridges, while others are associated with the tectonic processes by which pieces of oceanic lithosphere are thrust upon continental crust to form an ophiolite. As a result, fluids move through the formation through a complex set of crosscutting fractures containing alteration products from both modern, ongoing water–rock reactions, as well as hydrothermal processes during formation at the ridge axis.

The Oman Drilling Project, an activity under the auspices of the International Continental Scientific Drilling Program, has provided a unique opportunity to study peridotite aquifers by establishing a Multi-

* Corresponding author.
E-mail address: rsohn@whoi.edu (R.A. Sohn).

https://doi.org/10.1016/j.hydroa.2023.100163
Received 8 June 2023; Received in revised form 28 August 2023; Accepted 13 September 2023
Available online 20 September 2023

Borehole Observatory (MBO, Fig. 1) within a mantle section of the Samail ophiolite (Kelemen et al., 2021a). Four boreholes were established in 2018 at site BA1 within a ~ 100 m × 100 m region, and these holes have been comprehensively analyzed to characterize the site petrology, fluid chemistry, alteration history, hydrology (including pumping tests), and microbial activity (e.g., Katayama et al., 2020; Lods et al., 2020; Kelemen et al., 2021b; Nothaft et al., 2021, Ternieten et al., 2021). Here, we present water level data from two of the holes (BA1B, BA1D), which were monitored for a period of ~ 9 months in 2018. We analyze the water level response to tidal forcing (solid Earth tides, ocean tidal loads, and barometric pressure) and use the results to investigate the hydromechanical properties of the local peridotite aquifer. The amplitude and timing/phase of the water level response to these forcing mechanisms provides insight into the aquifer structure, and hydromechanical parameters such as storativity, transmissivity, and porosity, of the rocks surrounding the well bore (e.g., Bredehoeft, 1967; Hsieh et al., 1987; Rojstaczer and Agnew, 1989; Rojstaczer, 1988). Our analyses provide an opportunity to investigate the response of ophiolitic,

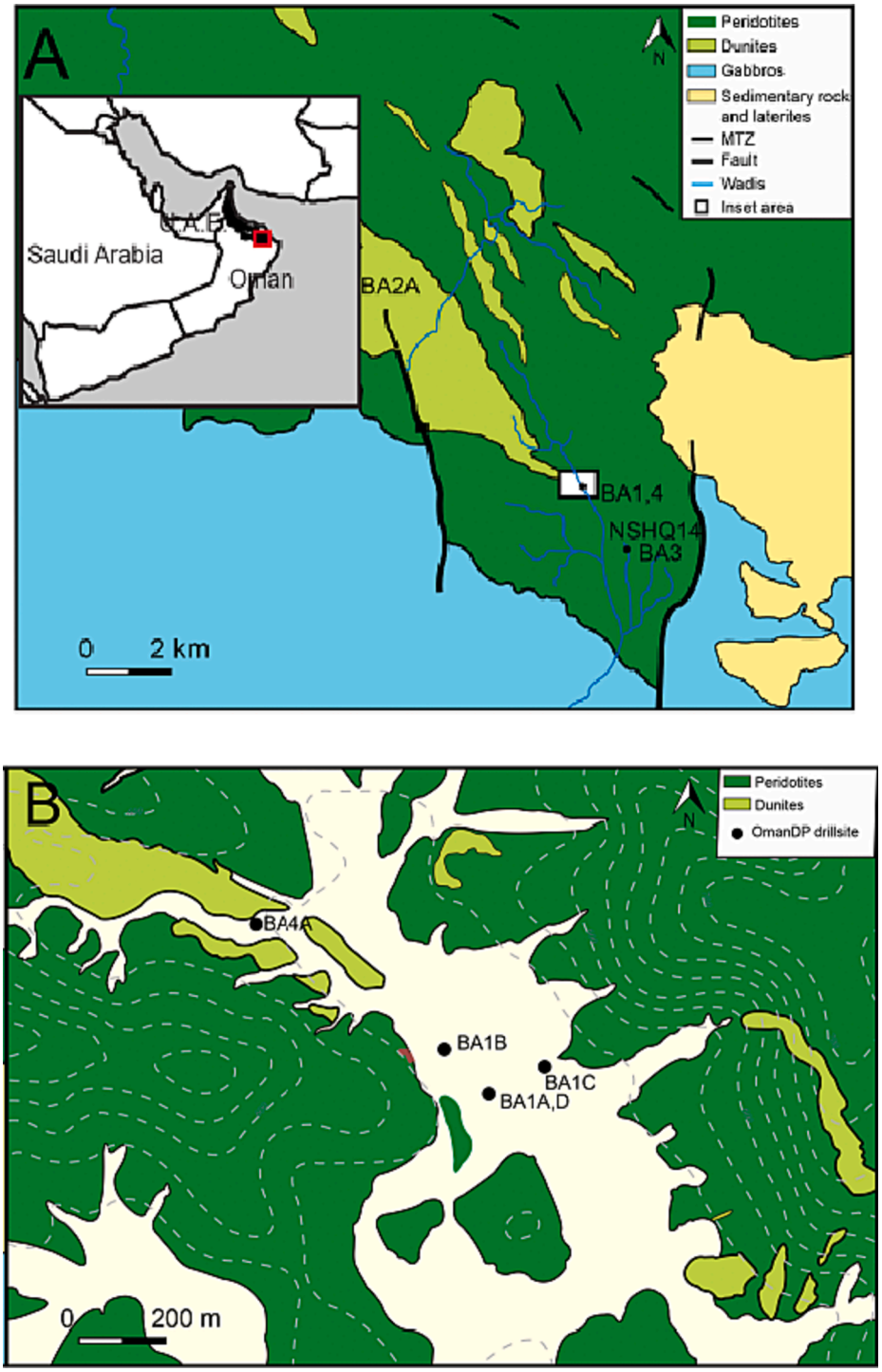

Fig. 1. Map of study area. (A) Inset: Location of Samail ophiolite in the northern part of Oman. Main: Zoom view of red box showing location of Multi-Borehole Observatory (MBO) experiment site (BA1,4) in the Samail ophiolite with local geology. (B) Detailed geology and borehole locations of the MBO. Data in this study is from holes BA1B and BA1D. (For interpretation of the references to colour in this figure legend, the reader is referred to the web version of this article.)

peridotite aquifers to tidal forcing, and to compare hydromechanical estimates derived from tidal analyses with those derived from pumping tests.

2. Site description

The host rocks of the MBO boreholes consist of partially, to almost completely, serpentinized dunites and residual harzburgites, with the degree of alteration generally decreasing with depth (Kelemen et al., 2021b). The site is located approximately in the middle of Wadi Lawayni, which is ~ 350 m wide at the MBO site and covered with a layer of gravel alluvium of variable thickness (0 - ~25 m). Like other parts of the Samail ophiolite, the upper ~ 40–50 m is highly fissured due to surface weathering (Dewandel et al., 2005). There is significant structural heterogeneity at the MBO, with a complex, cross-cutting vein structure, consisting of both carbonate and serpentine veins. The veins record a variety of fluid-rock reaction conditions, ranging from hydrothermal alteration near a mid-ocean ridge to present day subaerial weathering. The vein abundance generally decreases with depth in the holes, and carbonate veins are restricted to the upper few tens of meters.

The two holes that are the subjects of this study, BA1B and BA1D, were established using different methods. Hole BA1B was drilled using wireline diamond coring, which resulted in a hole diameter of 9.8 cm, and provided a nearly continuous ~ 400 m core for subsequent analyses. In contrast, Hole BA1D was drilled with an air rotary/hammer drill, which resulted in a hole diameter of 15.4 cm, and provided cuttings for subsequent analyses, but not continuous core samples. Lithological profiles of Holes BA1B and BA1D are shown in Fig. 2. Pumping/packer equipment were deployed in Hole BA1D, including cross-hole tests with nearby Hole BA1A (Fig. 1), to investigate their hydrological structure (Lods et al., 2020). The pumping tests demonstrated that the water table at Hole BA1D lies within a high conductivity zone that extends to a depth of ~ 75 m, with a productive interval at 26–27 m, and a partial confining layer overlying a low conductivity zone that extends to the bottom of the hole at 400 m (Fig. 3). These results indicate that Hole BA1D penetrates a low conductivity, partially confined aquifer overlain

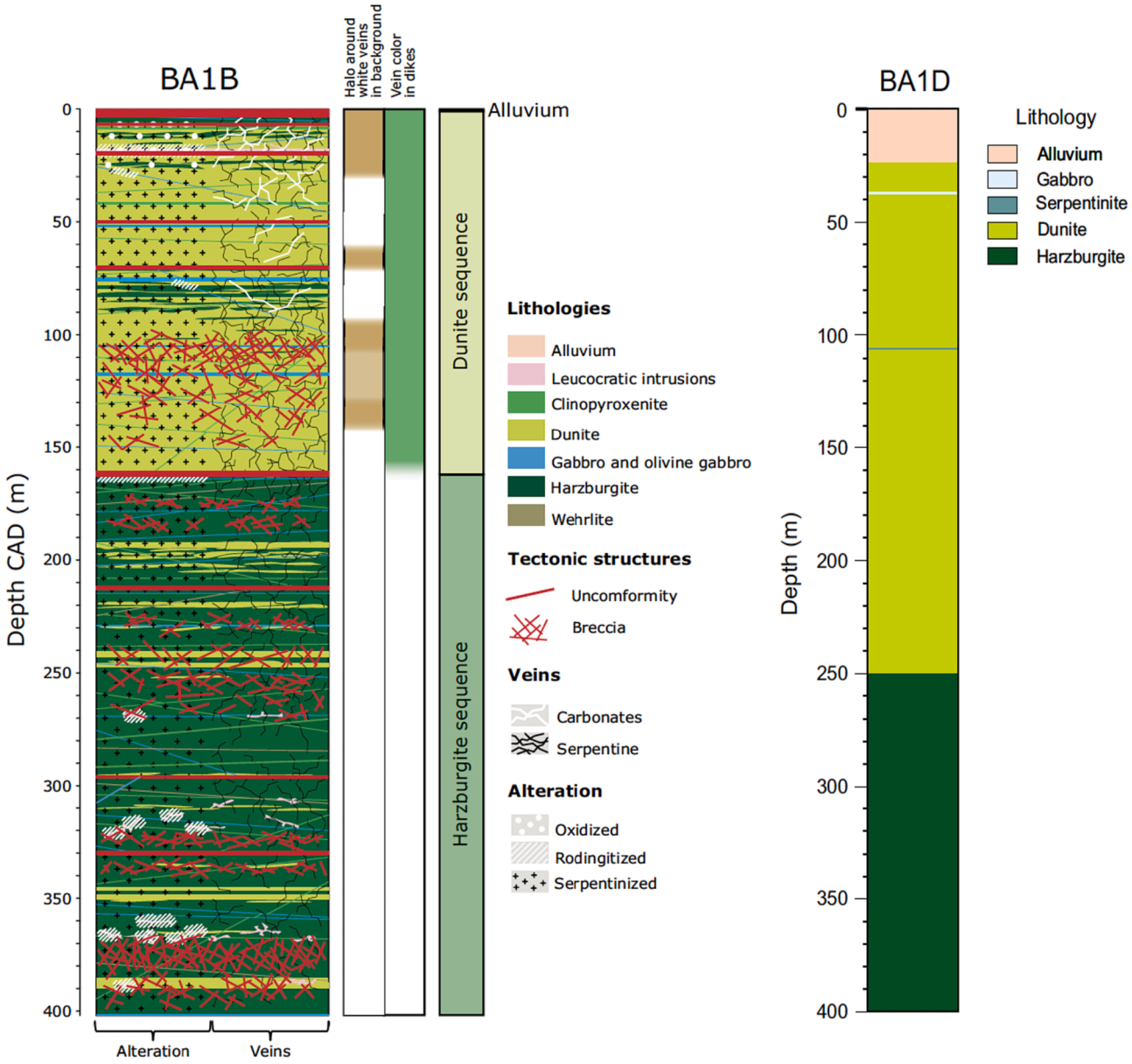

Fig. 2. Borehole lithologies, from Kelemen et al., (2021a). Hole BA1B is located at 22° 52.938′N, 58° 42.005′E, 583 m elevation. Hole BA1D is located at 22° 52.881′N, 58° 42.031′E, 584 m elevation.

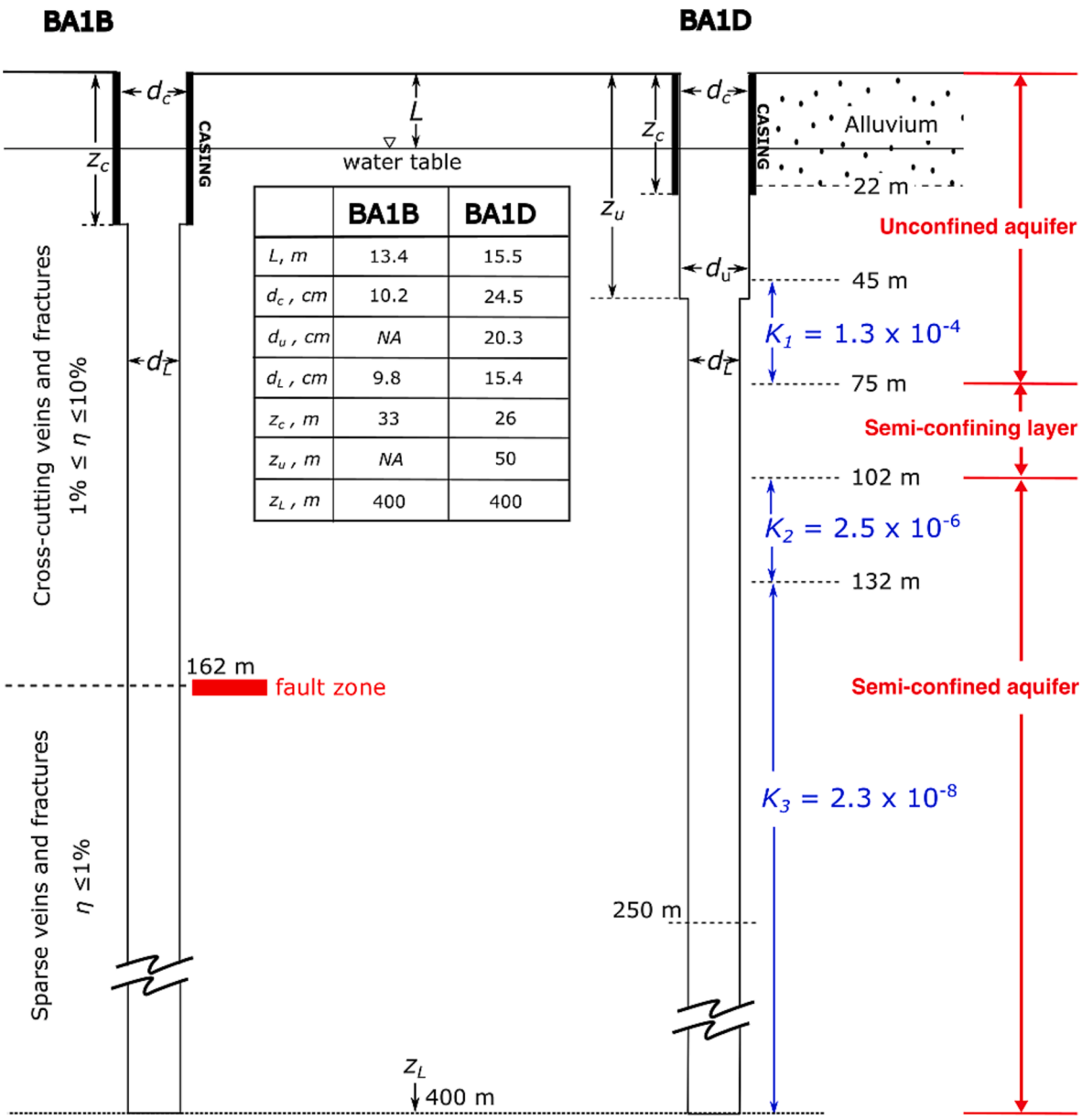

	BA1B	BA1D
L, m	13.4	15.5
d_c, cm	10.2	24.5
d_u, cm	NA	20.3
d_L, cm	9.8	15.4
z_c, m	33	26
z_u, m	NA	50
z_L, m	400	400

Fig. 3. Borehole schematics with dimensions in the inset table. Hydraulic conductivities in m s^{-1} from pumping tests (Lods et al., 2020) shown in blue for BA1D, and porosities from a resistivity survey (Katayama et al., 2020) are shown for BA1B. The conceptual aquifer structure for BA1D is shown in red. There are 22 m of alluvium above the hard rock at Hole BA1D, while at Hole BA1B there is no alluvium layer. A fault zone intersects Hole BA1B at a depth of 162 m. (For interpretation of the references to colour in this figure legend, the reader is referred to the web version of this article.)

by an unconfined water table aquifer. Pumping tests found evidence for vertical leakage across all the pumped/monitored intervals, and, overall, revealed a complex hydraulic system driven by multi-directional structural heterogeneities in the near-surface zone. The diameter of Hole BA1B was too small for the pumping equipment, but core sample analyses provide insight into its hydrologic structure (Kelemen et al., 2021b). Fracture/vein density and porosity are highest in the upper 162 m of the hole, which has a predominantly dunite lithology, with porosities ranging from zero to ~ 20%. A major fault zone intersects the hole at the 162 m depth interval, and below this horizon the porosities (less than1 %) and vein densities are much lower. The fault zone is ~ 3 m wide, dips at ~ 53°, and comprises multiple anastomosing and mutually cross-cutting shear planes, suggesting substantial strain accommodation with an inferred normal shear sense (Kelemen et al., 2021a).

3. Data and methods

We acquired water level and temperature data every 15 min from the BA1B and BA1D boreholes from April 2018 to January 2019 using Rugged TROLL® 100 non-vented (absolute) data loggers from *In-Situ Inc*. Contemporaneous atmospheric pressure and temperature data were acquired every 15 min at the BA1 site using a BaroTROLL® data logger from *In-Situ Inc*. The pressure data from the non-vented water level sensors were corrected by subtracting the atmospheric pressure data, and then converted to relative water level assuming a fluid density of 1000 kg m^{-3}. The water level data measure relative depth variations, and at the time of drilling in 2018 the water table was at an absolute depth of 13.4 m below the ground surface in Hole BA1B, and 15.5 m below the ground surface in Hole BA1D (Kelemen et al., 2021a). Earth tide (areal) strains at the study site were estimated using the *PyGTide* software (Rau, 2018). The sensor data and tidal strain estimates (Fig. 4)

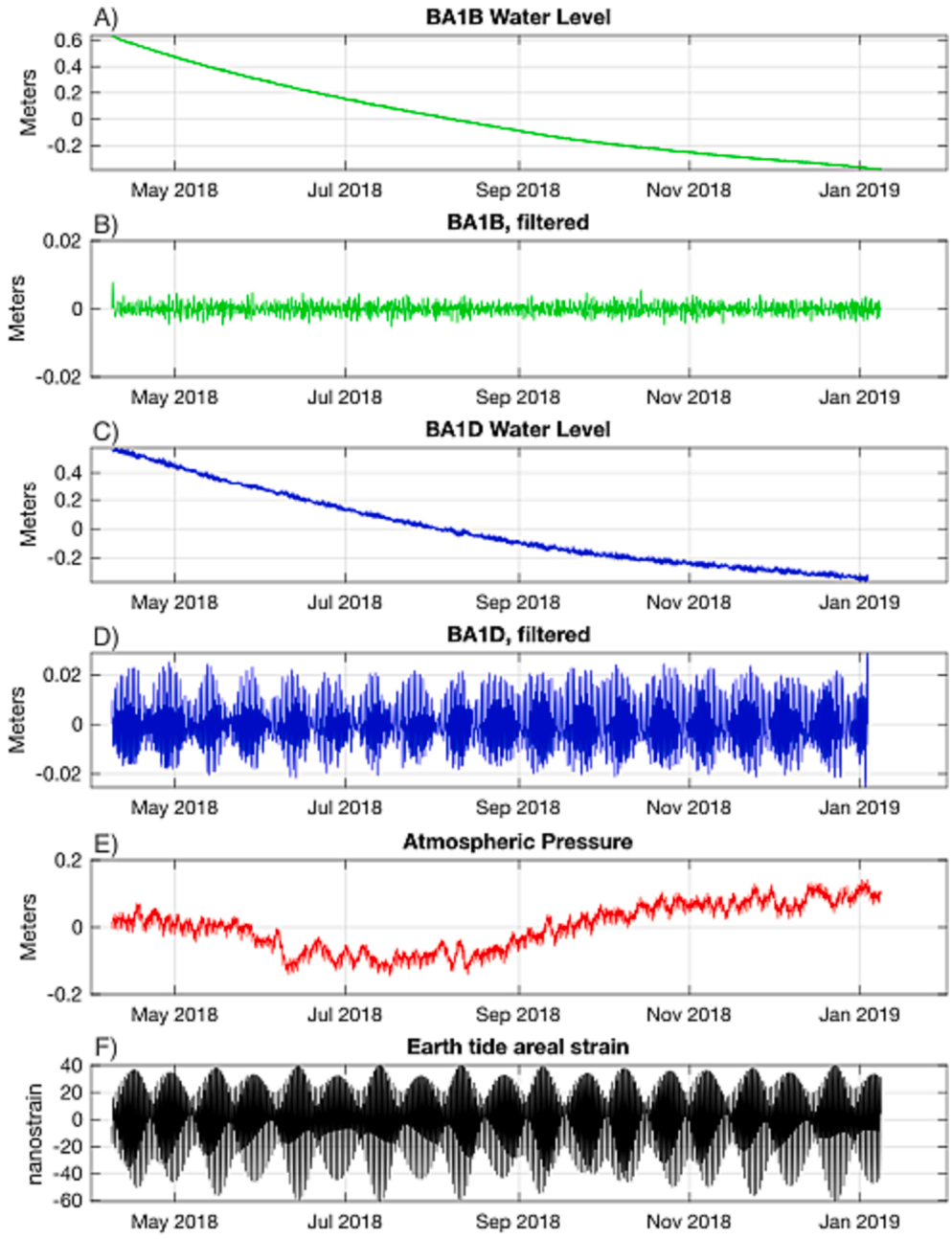

Fig. 4. Time-series data and Earth tide strain estimates used in this analysis. A) BA1B water level. B) BA1B bandpass filtered water level. C) BA1D water level. D) BA1D bandpass filtered water level. E) Atmospheric pressure. F) Earth tide areal strain. All time-series were sampled at 15 min. intervals and had their mean values removed. Atmospheric pressure data are expressed as meters of equivalent hydraulic head.

were acquired in local (UTC + 4) time coordinates and analyzed relative to Universal Time Coordinates (UTC).

Stochastic spectral estimates for each time-series were obtained using a multi-taper (time-bandwidth product = 3) method (Thomson, 1982) with adaptive weighting (Percival and Walden, 1993). Each time series was normalized to zero-mean, unit-variance prior to spectral estimation. The spectra (Fig. 5) of the earth tide and atmospheric pressure time-series exhibit the expected characteristics, with distinct peaks at the O1 (lunar declinational diurnal), K1 (luni-solar declinational diurnal), M2 (principal lunar semidiurnal), and S2 (principal solar semidiurnal) frequencies. The spectrum for water level at site BA1D exhibits peaks at all these same frequencies, whereas the spectrum for site BA1B does not have peaks at any of these frequencies, except possibly K1. Cross-spectral (multi-taper) coherency (C) estimates (Fig. 5) demonstrate that the water level variations at site BA1D are highly coherent with solid earth tides at the O1 ($C^2 = 0.93$) and M2 ($C^2 = 0.98$) frequencies, and with atmospheric tides at the K1 ($C^2 = 0.89$) and S2 ($C^2 = 0.99$) frequencies. In contrast, the water level variations at site BA1B are not highly coherent with any tidal forcing.

The amplitude and phase of the water level data, atmospheric pressure data, and Earth tidal strain estimates at the O1, K1, M2, and S2 frequencies were estimated by applying a robust, harmonic Least-Squares inversion (Chave, 2017) to the ~ 9-month records. All time-series were decimated to hourly sample intervals and filtered with a zero-phase, bandpass ($0.5 \leq f \leq 2.5$ cpd) filter prior to parameter estimation. Parameter uncertainties at the 95% confidence level were estimated using a non-parametric, bootstrap method with 100 replicates. The amplitude and phase estimates for the tidal components are shown in Fig. 6.

Oman boarders the ocean along its eastern and northern boundaries,

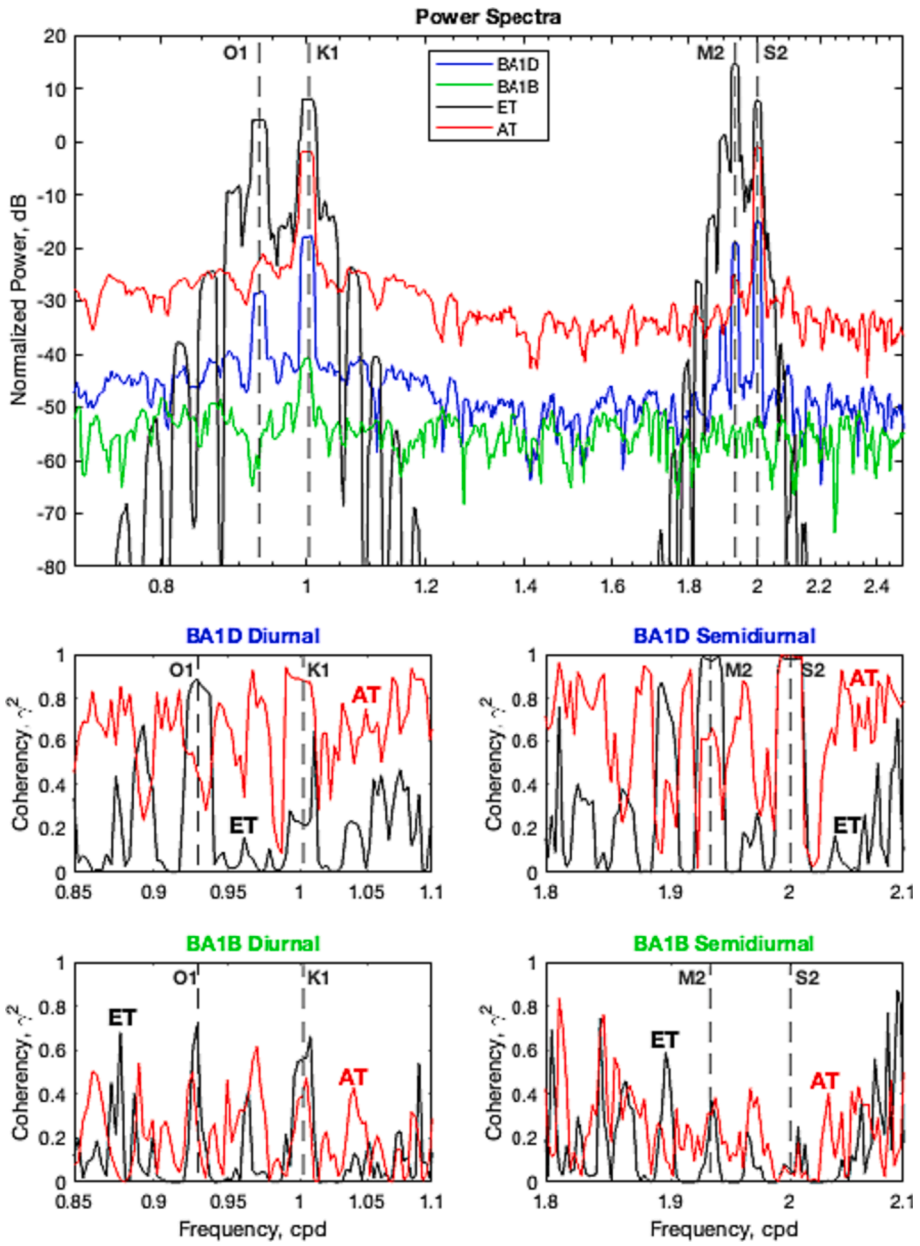

Fig. 5. Stochastic spectral estimates. Top panel: normalized power spectra for each time-series. Middle panels: Cross-spectral coherency between BA1D water level with atmospheric tides (red), and solid earth tides (black) at the diurnal (left panel) and semidiurnal (right panel) frequencies. Bottom panels: Same as middle panels but for BA1B water level. In all panels *x*-axis is frequency in cycles per day (cpd). (For interpretation of the references to colour in this figure legend, the reader is referred to the web version of this article.)

and the MBO site is ~ 42 km from the nearest coast. It is therefore necessary to consider the contribution of ocean tidal loading to crustal strain at the MBO site. We estimated areal strain due to ocean tidal loading using the *NLOADF* software, which convolves Green's functions for loading with calibrated ocean models to calculate geodetic parameters of interest for a given station location (Agnew, 1997). The areal strain amplitude and phase estimates for the MBO site due to ocean tidal loading, as well as the combined load from both solid Earth and ocean tides, are shown in Fig. 6 for the O1 and M2 frequencies. The amplitude and phase of the water level response relative to the imposed loads both with, and without, considering the effect of ocean tides are listed in Table 1. Barometric efficiencies at the K1 and S2 frequencies were estimated after 'disentangling' the response to solid Earth tides at the O1 and M2 frequencies (Rau et al., 2020), assuming negligible damping (i.e., $A^r_{K1} \approx A^r_{S2} \approx 1$, see Eq. 9 of Rau et al., 2020).

4. Discussion

We used spectral methods to estimate of the water level responses of two boreholes to tidal forcing, representing the first time, to our knowledge, that such an analysis has been conducted in a peridotite aquifer. The water level response to atmospheric (AT), solid Earth (ET), and ocean tides (OT) has implications for the geomechanical and hydrological structure of the surrounding aquifer (McMillan et al., 2019, and references therein). In the following sections we interpret the observed water level responses for the two boreholes, derive hydromechanical parameter estimates for the formation surrounding the boreholes where possible, and compare our estimates with those derived from pumping tests.

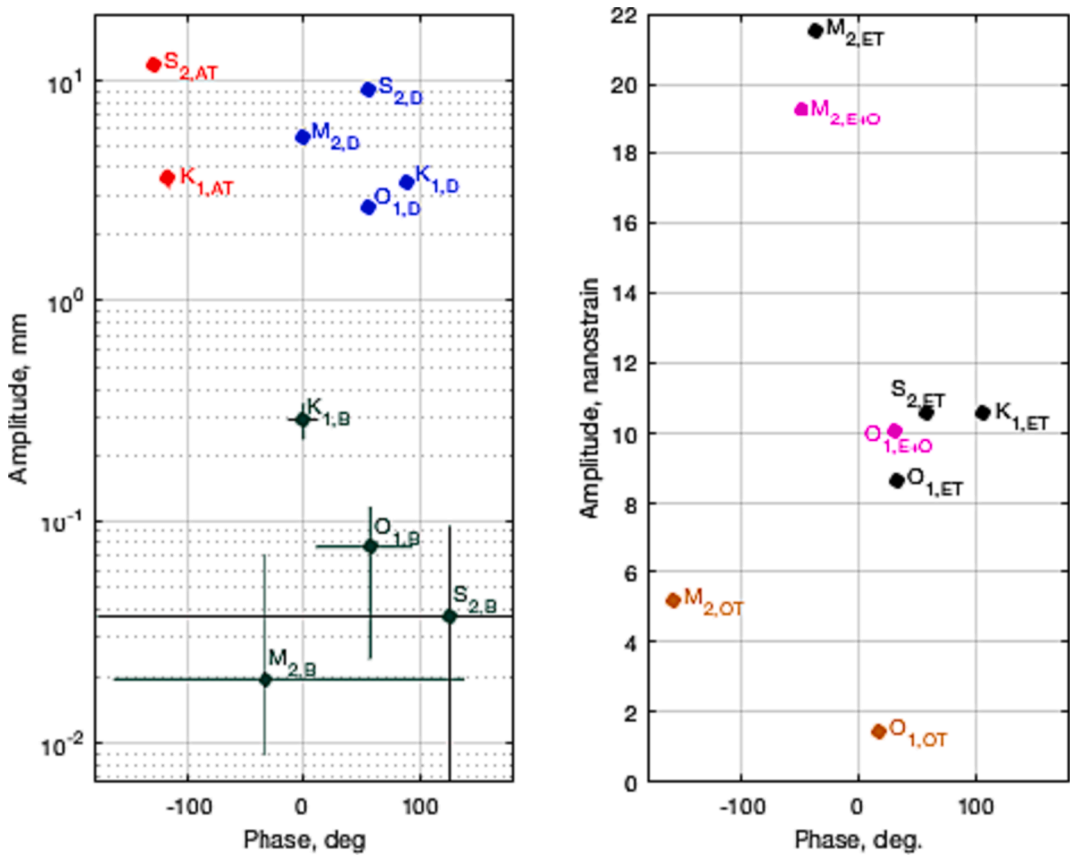

Fig. 6. Amplitude and phase of the tidal components. Left panel: Water levels in Hole BA1B (dark green), Hole BA1D (blue), and local atmospheric pressure expressed in equivalent head (red). A logarithmic *y*-axis is used to display the full range of observed variations. Right panel: Areal strain estimates for the MBO site induced by solid Earth tides (black, ET), ocean tidal loading (dark orange, OT), and the combination of the two (magenta, ET + OT). 95% confidence intervals for parameter estimates are shown with solid lines. Where the lines cannot be seen, the confidence intervals are smaller than the symbols. All phase estimates are relative to UTC. (For interpretation of the references to colour in this figure legend, the reader is referred to the web version of this article.)

Table 1
Amplitude and phase response of borehole water level to tidal forcing. Two sets of values are shown for each borehole: (ET, AT) = loading from solid Earth and atmospheric tides, (ET + OT, AT) = loading including ocean tides. Response to areal strain expressed in mm per nanostrain (mm/nε). Response to atmospheric pressure expressed as barometric efficiency (*BE*). A negative phase lag means water level response lags tidal forcing. The ± values represent the 95% confidence intervals of the parameter estimates.

Frequency (cpd)	**BA1B**			**BA1D**		
	ET, AT	**ET + OT, AT**	**Uncert**	**ET, AT**	**ET + OT, AT**	**Uncert**
	Amplitude Response (±95% confidence intervals)					
O1	0.01 mm/nε	0.01 mm/nε	±0.01	0.31 mm/nε	0.26 mm/nε	±0.03
M2	0.00 mm/nε	0.00 mm/nε	±0.00	0.25 mm/nε	0.28 mm/nε	±0.01
BE_{K1}^{AT}	0.10	0.10	±0.02	0.63	0.64	±0.05
BE_{S2}^{AT}	0.00	0.00	±0.00	0.61	0.64	±0.02
	Phase Lag, deg., (95% confidence intervals)					
O1	−23.2	−25.6	±39.1	−21.7	−24.0	±3.9
M2	−1.4	−14.6	±170.6	−35.1	−48.2	±2.3
BE_{K1}^{AT}	−105.5	−107.2	±12.1	−139.3	−151.2	±5.8
BE_{S2}^{AT}	87.5	90.1	±177.4	−173.1	−168.5	±1.9

4.1. *Interpreting the observed borehole responses to tidal forcing*

The most striking and robust aspect of our results is that the two boreholes in this study have dramatically different responses to tidal forcing, despite being separated by a lateral distance of only ~ 100 m. The contrasting responses imply substantial, short length scale lateral heterogeneity in the local aquifer structure. The ophiolitic rocks are extensively fractured due to both mid-ocean ridge accretionary processes and the tectonic processes associated with obduction onto the continental plate, and the surface rocks are further fractured due to weathering (Dewandel et al., 2005). The hydrological structure of the MBO site is strongly affected by these multi-directional faults and fractures, which produce lateral heterogeneity, and provide high conductivity pathways for fluid flow (Lods et al., 2020).

We can assess the potential impact of structural heterogeneity on the response to tidal forcing by considering that the induced flow is limited to a discrete volume surrounding the borehole with a radius of approximately $\sqrt{\kappa\tau}$, where κ is the formation hydraulic diffusivity (L^2/T), and τ is the tidal period (T). The observed response thus averages the aquifer properties within a cylinder whose radius depends on lateral diffusivity and the timescale of forcing. Pumping tests in Hole BA1D (Lods et al., 2020) provided an estimate of hydraulic conductivity, K, (4.5×10^{-6} m/s) and the specific storage, S_s, (1.35×10^{-4} m^{-1}) averaged over the entire hole. Using the relation $\kappa = K/S_s$, we obtain a hole-averaged diffusivity estimate of 3.3×10^{-2} m^2/s. Using this value, the relevant lateral length scales for the tidal response are ~ 55 m and ~ 38 m at the diurnal, and semi-diurnal, periods, respectively. These length scales are smaller than the offset distance between Holes BA1B and

BA1D, indicating that their tidal responses sample distinct, non-overlapping portions of the formation. These length scales are larger, however, than the offset distance (~15 m) between Holes BA1A and BA1D, which exhibited different hydrological responses to pumping (Lods et al., 2020), indicating that the tidal responses may sample heterogeneous structures. This affects our ability to model our observations since a laterally uniform formation is typically assumed when tidal responses are interpreted. If the tidal response is driven by the deep, low porosity portion of the formation, which yielded a conductivity estimate of 2.3×10^{-8} m/s from pumping tests, then the length scales decrease to values less than 5 m for both the diurnal and semi-diurnal periods. In this case the assumption of lateral uniformity for modeling the borehole water level response to tidal loading may be justified.

The water level response in a borehole to tidal loading depends on a variety of factors, including the aquifer's structure (confined vs. unconfined), its elastic properties, the pneumatic and hydraulic behavior of the unsaturated zone, the borehole depth, and in some cases channelized fracture flow, capillary effects, and well bore storage and skin effects (Bredehoeft, 1967; Van der Kamp and Gale, 1983; Bower, 1983; Hsieh et al., 1987; Rojstaczer, 1988; Rojstaczer and Agnew, 1989; Cutillo and Brehehoeft, 2011; Wang et al., 2018; Liang et al., 2022; Zhang et al., 2023). These complexities present challenges for modeling and interpreting our results, but our interpretation for Hole BA1B is relatively straightforward. A lack of response to tidal strain indicates that the aquifer fluids are likely not under pressure due to confinement (we revisit this assumption, below), while a lack of response to barometric loading indicates that there is no pressure imbalance between the water level surface in the well and the local water table. Since the water level surface in an open well is pressurized instantaneously by barometric pressure while the pressure load at the water table can be delayed and/or attenuated by pneumatic diffusion through the unsaturated zone (Weeks, 1979), a lack of response to barometric loading further requires that the surficial rocks comprising the unsaturated zone have a high pneumatic diffusivity. We thus conclude that Hole BA1B penetrates a locally unconfined aquifer overlain by a fractured/weathered unsaturated zone with high pneumatic diffusivity. One of the primary structural differences between the two wells in this study is that Hole BA1B is intersected by a ~ 3 m thick fault zone at a depth of 162 m (Kelemen et al., 2021a). The fault zone, dipping at 53°, could provide a high conductivity pathway to the water table and this may contribute to the apparent unconfined behavior of the local aquifer.

The water levels in Hole BA1D exhibit robust responses to both tidal strain and barometric pressure, suggesting at least some degree of confinement. The water level in an unconfined well is only expected to respond to tidal strain under a narrow set of conditions (Bredehoeft, 1967; Rojstaczer and Riley, 1990), and assuming well bore storage effects are negligible and uniform aquifer properties, the sensitivity can be expressed as a dimensionless water table parameter, Ω' (Rojstaczer and Riley, 1990). The water table parameter is a function of the aquifer thickness (Bredehoeft, 1967), and for an infinitely thick aquifer (maximum sensitivity), the amplitude sensitivity of the water table to tidal strain can be expressed as (Rojstaczer and Riley, 1990):

$$\frac{\Omega'}{(1-i)} = \sqrt{\frac{S_s K_z}{2 S_y{}^2 \omega}} \tag{1}$$

where K_z is vertical hydraulic diffusivity (L T^{-1}), S_y is specific yield (–), and ω is the frequency of forcing (T^{-1}). A significant response to Earth tides is only expected for aquifers with high (vertically averaged) values of S_s and K_z, and low values of S_y. Using the hole-averaged estimates of S_s and K_z derived from pumping tests (Lods et al., 2020), and assuming that specific yield is similar to that estimated for fractured granitic aquifers ($10^{-3} \leq S_y \leq 10^{-2}$, Marechal et al., 2003; Marechal et al., 2006), the amplitude sensitivity of Hole BA1D to tidal strain assuming unconfined conditions is a small number on the order of 10^{-2} to 10^{-1}. These values indicate that if Hole BA1D penetrates an unconfined aquifer, the water level would not be expected to respond to tidal strain.

4.1.1. Amplitude response to tidal strain

For a semi-confined aquifer, the amplitude response to tidal strain can be used to estimate the elastic properties of the aquifer rock, while the phase lag can be used to estimate aquifer hydraulic properties (e.g, Cutillo and Brehehoeft, 2011), assuming undrained conditions are met (Bastias Espejo et al., 2022). Before attempting to model the response parameters we must consider that the MBO site is only ~ 42 km from the nearest coast, such that ocean tidal loading may be expected to impact crustal strain. The areal strain amplitude from ocean tidal loading at the MBO site is estimated to be ~ 20% that due to solid Earth tides at the O1 and M2 frequencies, with constructive interference at the O1 frequency, and destructive interference at the M2 frequency (Fig. 6). Our estimates of water level sensitivity to areal strain (Table 1) thus depend on whether we include the applied strain from ocean tidal loading. We address this issue by modeling the borehole water level response to applied strain under both scenarios (i.e., ET only, ET + OT), and then compare parameter estimates to assess the impact of ocean tidal loading.

We must also consider the fact that short length scale structural heterogeneities and channelized fracture flow, both of which may be important for the hydraulic behavior of the formation around Hole BA1D, may affect the water level response to tidal forcing. We cannot formally include these factors in our analysis because none of the existing models for water level response to tidal forcing allow for lateral heterogeneity and channelized flow in multi-directional fractures. We must therefore estimate hydromechanical parameters using simplified models, and these estimates can then be compared with those obtained via other methods (e.g., pumping) to provide insight into how the unmodeled complexities affect parameter estimates.

We begin by following the approach of Rojstaczer and Agnew (1989) to interpret the amplitude response to tidal strain. This model assumes: 1) uniform hydromechanical properties of the aquifer (no lateral variability), 2) well bore storage is negligible (static-confined conditions), and 3) no vertical fluid flow between the well intake and the water table above. An iterative method is used to estimate the formation compressibility, specific storage, and porosity, based on the amplitude sensitivity to areal strain at the O1 and M2 frequencies. The formation compressibility (β) is expressed as a function of the amplitude sensitivity to areal strain (A_s', meters/unit strain), and the constant parameters required to begin the iterative solution are gravitational acceleration, fluid density, fluid compressibility, the formation loading efficiency (γ), and the Poisson's ratio (ν) and (undrained), grain-scale compressibility (β_u) of the aquifer rock (Table 2). The wall rocks of well BA1D (Fig. 2) are dominantly fractured dunite from the bottom of the well casing (22 m) to 250 m, and fractured harzburgite from 250 to 400 m. All of this peridotite is altered, with the degree of alteration generally decreasing with depth in the hole (Kelemen et al., 2021b). The elastic properties of the aquifer rock (i.e., serpentinite) depends strongly on the degree of alteration (Christensen, 1966), and in this analysis we use a Poisson's ratio of 0.35 and a grain-scale compressibility of 6×10^{-11} Pa^{-1} based on laboratory measurements (Christensen, 1996; 1996; Falcon-Suarez et al., 2017). We estimate the formation loading efficiency as one minus the barometric efficiency (Van der Kamp and Gale, 1983).

The iterative procedure begins with an initial guess for the formation compressibility (1×10^{-10} Pa^{-1}), and then cycles through a set of equations that update this estimate (see Eq. (2), 18, and 19 in Rojstaczer and Agnew, 1989) until it converges to a stable value. Once a final estimate for β is obtained, the corresponding porosity (η) and specific storage (S_s) of the formation can be estimated (see equations 20 and 26 in Rojstaczer and Agnew, 1989). Following this procedure, we obtain estimates for the elastic properties of the aquifer rock. For the ET + OT scenario, the responses at the O1 and M2 frequencies are within error at the 95% confidence level, suggesting that a static-confined response was observed. Using the M2 frequency response (0.28 mm/n ε), we obtain

Table 2
Hydromechanical parameters for Hole BA1D. Fixed parameters were held constant during the analysis. Modeled parameters represent estimates providing the best-fit to the observed tidal responses (Table 1) using the models described in the text.

Parameters		Scenario		
Fixed parameters		ET + OT Applied Strain	ET Applied Strain	AT Barometric Load
g, gravity acceleration ($m/s^{-2}(-\|-)$)	9.81			
ρ_f, fluid density (kg m^{-3})	998			
β_f, fluid compressibility (Pa^{-1})	4.59×10^{-10}			
ν, Poisson's ratio	0.35			
β_u, solid compressibility (Pa^{-1})	6×10^{-11}			
b, well penetration length, (m)	298			
b', confining layer thickness (m)	27			
r_c, well casing radius (m)	0.102			
r_w, open well radius (m)	0.077			
Modeled parameters				
γ, Loading efficiency (–)				0.36
D_a, unsaturated zone pneumatic diffusivity (m^2/s)				$>5 \times 10^{-2}$
K', confining layer vertical conductivity (m/s)		3.5×10^{-8}	0	5.0×10^{-9}
S', confining layer storage coefficient (–)				7.0×10^{-6}
β, matrix compressibility (Pa^{-1})		6.8×10^{-11}	8.4×10^{-11}	
η, aquifer porosity (–)		0.03	0.08	
K, aquifer hydraulic conductivity (m/s)		6.7×10^{-9}	1.6×10^{-8}	4.0×10^{-6}
S_s, aquifer specific storage (m^{-1})		1.9×10^{-7}	5.4×10^{-7}	
S, aquifer storage coefficient (–)		5.8×10^{-5}	1.6×10^{-4}	7.0×10^{-6}
T, aquifer transmissivity (m^2/s)		2.0×10^{-6}	4.8×10^{-6}	

parameter estimates for matrix compressibility, porosity, and specific storage (Table 2). We obtain a second set of parameter estimates for the M2 response in the ET only scenario (0.25 mm/n ϵ), with a porosity and specific storage that are about 2.5 times larger than those obtained for the ET + OT scenario.

4.1.2. Phase response to tidal strain

We follow the approach of Wang et al. (2018) to model the phase response of hole BA1D to applied strain. The Wang et al. (2018) model builds upon previous work by Hsieh et al. (1987) by including vertical leakage through a semi-confining layer, which is appropriate for the aquifer structure at Hole BA1D (Lods et al., 2020). The model consists of an aquifer overlain by a semi-confining aquitard that is overlain by an unconfined aquifer, and it assumes: 1) the aquifer is isotropic, homogeneous, and of large lateral extent, 2) inertial effects of water in the well bore are negligible, and 3) purely vertical flow through an incompressible aquitard with zero storage. The degree of leakage is quantified by the parameter K'/b', where K' and b' are the vertical hydraulic conductivity and thickness of the aquitard, respectively. The phase lag is given by:

$$\phi = arg\left[\frac{i\omega S}{(i\omega S + K'/b')\xi}\right] \tag{2}$$

$$\xi = 1 + \left(\frac{r_c}{r_w}\right)^2 \frac{i\omega r_w K_0(\beta r_w)}{2T\beta K_1(\beta r_w)} \tag{3}$$

$$\beta = \left(\frac{K'}{Tb'} + \frac{i\omega S}{T}\right)^{1/2} \tag{4}$$

where T is the aquifer transmissivity, S is the storage coefficient, ω is the forcing frequency, r_c is the well casing radius, r_w is the radius of the open portion of the well, K_0 is the zeroth order modified Bessel function of the second kind, and K_1 is the first order modified Bessel function of the second kind. The storage coefficient can be estimated using the values of specific storage obtained above, since $S = S_s b$, where b is the thickness of the portion of the well that penetrates the aquifer. Pumping tests indicate that the bottom of the semi-confining layer is at a depth of ~ 102 m, yielding b = 298 m. Using the values of S_s obtained in our amplitude response analysis, above, we obtain $S = 5.8 \times 10^{-5}$ and $S = 1.6 \times 10^{-4}$ for the ET + OT and ET only scenarios, respectively. We then use forward modeling to obtain estimates of aquifer transmissivity and leakage parameter that match the observed phase lags at both the O1 and M2 frequencies (Table 1), yielding $T = 2.0 \times 10^{-6}$ m^2/s, $K'/b' = 1.3 \times 10^{-9}$ s^{-1} for the ET + OT scenario and $T = 4.8 \times 10^{-6}$ m^2/s, $K'/b' = 0$ for the ET scenario. This, in turn, allows us to estimate the hydraulic conductivity (K) of the aquifer, since $K = T/b$, yielding $K = 6.71 \times 10^{-9}$ m/s and 1.61×10^{-8} m/s [1]for the ET + OT and ET only scenarios, respectively (Table 2). Finally, for a partial confining layer that extends from 75 to 102 m depth, b'= 27 m and we can estimate the vertical conductivity of the confining layer based on the leakage parameter estimates (Table 2).

4.1.3. Response to barometric loading

The amplitude of the water level response to barometric forcing is expressed through the barometric efficiency (*BE*), which is the ratio between the amplitude of the water level response and the equivalent head of the atmospheric pressure changes (Clark, 1967). If the confining layer is impermeable and the aquifer transmissivity is high, the *BE* would be one minus the loading efficiency and the phase lag would −180° for all frequencies of atmospheric loading (Rojstaczer, 1988). If, however, the confining layer is permeable and/or the aquifer transmissivity is low, then both *BE* and phase will be a function of frequency. This leads to the concept of barometric response functions, which can be expressed as either a function of frequency or time lag (e.g., Rojstaczer, 1988; Furbish, 1991; Rasmussen and Crawford, 1997).

We were only able to obtain robust gain and phase lag estimates for the barometric response at the K1 and S2 frequencies, but we can nevertheless attempt to model these observations. Assuming that: 1) the aquifer and partial confining layer have the same undrained response to surface loading, 2) air flow between the Earth's surface and the water table is vertical, and 3) groundwater flow between the aquifer and borehole is horizontal, the problem can be decoupled into three discrete flow problems: 1) vertical air flow between the Earth's surface and the water table, 2) vertical groundwater flow between the water table and the aquifer, and 3) horizontal groundwater flow between the aquifer and borehole with concomitant leakance (Rojstaczer, 1988).

The impact of these processes on the water level response can be expressed through the dimensionless frequencies (Rojstaczer, 1988):

$$R = L^2\omega/2D_a, \text{ unsaturated zone frequency} \tag{6}$$

$$q = b'\omega/K', \text{ partial confining layer frequency} \tag{7}$$

and

$$W = \omega r_w^2/Kb, \text{ aquifer frequency} \tag{8}$$

where L is the water table depth, b' is the partial confining layer thickness, and K' is the vertical hydraulic conductivity of the partial confining layer.

Since the water table is at a relatively shallow depth and the unsaturated zone at Hole BA1D is comprised of a weathered and fractured

surficial layer, it seems reasonable to assume, consistent with our interpretation for Hole BA1B, that pressure at the water table equals that at the water surface in the well. The diffusion of the pressure load to the aquifer is decoupled from unsaturated zone effects when $R/q \ll 1$, and the water level response is controlled by vertical groundwater flow through the partial confining layer and horizontal flow between the aquifer and borehole. The impact of these two processes on the barometric response is determined by the ratio $qS'/2W$, where S' is the confining layer storage coefficient (Rojstaczer, 1988). Assuming the bottom of the partial confining layer (b') is at a depth of 87 m (Lods et al., 2020), then the key unknown parameters are K', S', and K.

Our analysis yielded a constant value of $BE = 0.64$ for both the K1 and S2 frequencies, but with different phase lags (K1 $= -151.2 \pm 5.8°$, S2 $= -168.5 \pm 1.9°$). Constant amplitudes at the K1 and S2 frequency implies static-confined conditions, but the large phase lag difference ($\sim 17°$) is inconsistent with this interpretation. We performed a grid-search over the plausible parameter space ($10^{-10} \leq (K', K) \leq 10^{-5}$ m/s, $10^{-6} \leq S \leq 10^{-2}$) to find the combination of K', S', and K that provide the best fit to our observations for Hole BA1D. We found that there is no part of the plausible solution space where the amplitude response at the K1 and S2 frequencies is the same within error while the phase lag at the S2 frequency is 17° larger than the K1 frequency. As a result, none of the parameter combinations were able to fit the observations to within the 95% confidence intervals. Our best-fitting model (Fig. 7) yielded values of $K' = 5 \times 10^{-9}$ m/s, $K = 4 \times 10^{-6}$ m/s, and $S = S' = 7 \times 10^{-6}$.

In our analysis of the response to barometric loading we assumed that pore pressure damping effects at both the K1 and S2 frequencies are negligible (i.e., $A^r_{K1} \approx A^r_{S2} \approx 1$). Since the observed responses to areal strain are equal within error at the O1 and M2 frequencies, it is reasonable to assume that $A^r_{K1} \approx A^r_{S2}$, but the values may be less than one. It is thus possible that our barometric efficiency estimates are too low, but this would not resolve our modeling issue so long as the response to barometric loading has equal amplitudes but significantly different phase lags at the K1 and S2 frequencies.

4.2. Evaluation of parameter estimates and comparison with pumping test results

Multi-level pumping/packer tests conducted at Hole BA1D yielded hydromechanical parameter estimates (Lods et al., 2020) that we can compare with our estimates based on the water level response to tidal loading. The pumping test results yielded a three-layer hydraulic structure (Fig. 3), with a high conductivity surficial layer ($K = 1.3 \times 10^{-4}$ m/s) extending to a depth of $\sim$ 75 m, underlain by a lower conductivity partial confining layer. Beneath the partial confining layer is a low conductivity aquifer ($K = 2.3 \times 10^{-8}$ m/s) with a higher conductivity ($K = 2.5 \times 10^{-6}$ m/s) cap. The pumping tests also revealed evidence for vertical leakance across all layer boundaries.

The aquifer transmissivity/conductivity estimates we obtained by applying the model of Wang et al., (2018) for the phase lag of the water level response to applied strain ($K = 6.71 \times 10^{-9}$ m/s) are about a factor of three lower than the pumping test estimates. This agreement is reasonable considering that the model assumes a laterally extensive and isotropic aquifer, and the implication is that the water level response to applied strain is controlled by a cylindrical volume of rock with an outer radius of several meters surrounding the deep, low conductivity, portion of the borehole. The pumping tests did not provide aquifer compressibility, porosity, and specific storage estimates to directly compare with those we obtained based on the amplitude response to applied strain using the model of Rojstaczer and Agnew (1989). However, a downhole resistivity survey of Hole BA1B, returned porosity estimates of a few percent at depths below $\sim$ 50 m, and a few tenths of a percent at depths

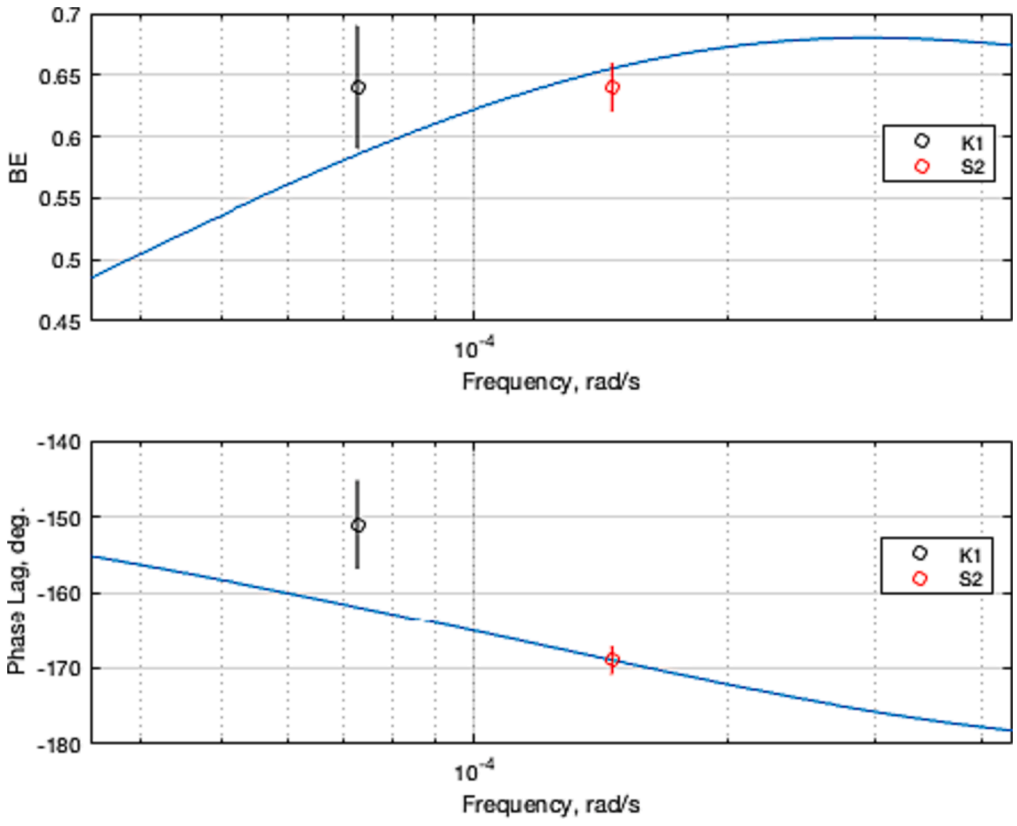

Fig. 7. Modeled vs. observed barometric response for Hole BA1D. The vertical lines show the 95% confidence intervals for each observation. The blue curve is the best-fitting (L2 norm, misfit weighted by inverse of uncertainty) barometric response function assuming $R/q \ll 1$ ($D_a > 5 \times 10^{-2}$ m^2 s^{-1}) for a grid search over the parameter space $10^{-10} \leq (K', K) \leq 10^{-5}$ m s^{-1}, $10^{-6} \leq S \leq 10^{-2}$. (For interpretation of the references to colour in this figure legend, the reader is referred to the web version of this article.)

below 162 m (Katayama et al., 2020). For comparison, we obtained an aquifer porosity estimate of 3% based on the response to the total (ET + OT) applied strain, and 8% if we only consider strain from the solid Earth tide (ET).

Our hydromechanical parameter estimates using the model of Rojstaczer (1988) for the water level response to barometric loading are more difficult to interpret because we were not able to reproduce our observations to within error. Our best-fitting model for the barometric response consists of a relatively high conductivity aquifer (4×10^{-6} m/s) overlain by a low conductivity confining layer (5×10^{-9} m/s). This aquifer conductivity estimate is similar to the pumping test conductivity estimate for the upper part of the semi-confined aquifer (2.5×10^{-6} m/s), but much higher than the estimate for the lower part of the aquifer (2.3×10^{-8} m/s). This suggests that the water level response to barometric loading may be driven by flow just beneath the partial confining layer, but the lack of a good-fitting model precludes a definitive interpretation.

Our ability to adequately model the response to applied strain but not barometric loading may be due the different ways they affect the formation pore pressure. Barometric loading is a top-down phenomenon and pressure variations must diffuse from the ground surface to the aquifer. The hydrologic structure at Hole BA1D above the partial confining layer is complex and characterized by channelized flow in multi-directional fractures (Lods et al., 2020), whereas it is an isotropic medium in the model. We may therefore expect the downward diffusion of barometric pressure variations to differ substantially from the model assumptions, providing a plausible explanation for the inability of the model to reproduce the amplitude and phase lag observations. By contrast, tidal strain variations are instantaneous at all depths, and low porosity zones will generate the largest pore pressure perturbations. The response to tidal strain may therefore be driven by the deep, low porosity/conductivity part of the borehole, with the complex near surface zone having at most a second-order effect.

The magnitude of the applied strain from ocean tidal loading at the MBO site, which is ~ 42 km from the nearest coast, is estimated to be ~ 20% that due to solid Earth tides. Including the ocean tidal load in the applied strain estimate rectifies the amplitude response at the O1 and M2 frequencies to within error of static-confined, whereas there is a ~ 25% difference at these frequencies when the ocean tidal load is neglected. Many of the aquifer hydromechanical parameter estimates (T, S_s, η) for the ET scenario are about 2.5 times larger than those obtained for the ET + OT scenario but we don't have enough information to determine which set of estimates is more accurate. However, the leakage parameter (K'/b') estimate of 1.3×10^{-9} s^{-1} obtained from phase lag modeling for the ET + OT scenario is consistent with the pumping test results, which provided robust evidence for vertical leakage across all layers (Lods et al., 2020), whereas the leakage estimate of zero for the ET scenario, which implies a perfectly confined aquifer, is not. This provides an indication that failing to account for ocean tidal loading can lead to significant errors when analyzing water level responses in boreholes near coastlines. More research is needed to understand how ocean tidal loading affects the response of borehole water levels to applied strain, and this could be facilitated by directly measuring strain, instead of estimating it, in boreholes near coastlines.

5. Conclusions

We present water level and atmospheric pressure data acquired from two boreholes established in a peridotite aquifer, and, in combination with applied strain estimates from solid Earth and ocean tides, use the data to analyze the borehole water level response to tidal forcing. Our results, which examine how the aquifer responds to long-wavelength periodic loading, are complementary to the pumping test results of Lods et al. (2020) and provide an opportunity to compare hydromechanical estimates obtained using different techniques.

1) Our most robust result is a high degree of lateral heterogeneity in the aquifer structure, with two wells separated by ~ 100 m exhibiting markedly different responses to tidal forcing. The water level in Hole BA1B does not respond to either tidal strain or atmospheric pressure, while the water level in Hole BA1D responds to both. This phenomenology indicates that Hole BA1B penetrates an unconfined aquifer, while Hole BA1D penetrates an aquifer with some degree of confinement. This high degree of lateral heterogeneity is consistent with pumping test results.
2) The water level response to tidal strain observed in Hole BA1D can largely be explained using partially-confined aquifer models, yielding estimates for the bulk compressibility (6.65×10^{-11} Pa^{-1}), porosity (3%), specific storage (1.9×10^{-7} m), and transmissivity/conductivity (2.0×10^{-6} m^2/s/6.7×10^{-9} m/s) of the aquifer. The conductivity and porosity estimates are within a factor of about 2–3 of those derived from pumping tests and a downhole resistivity survey.
3) The water level response to barometric loading observed in Hole BA1D cannot be adequately explained with simple aquifer models, likely due to the complex hydraulic structure of the near-surface zone.
4) The applied strain from ocean tidal loading at the MBO site, which is ~ 42 km from the nearest coast, is estimated to be ~ 20% of that due to solid Earth tides. Including ocean tidal loading in the applied strain estimate rectifies the amplitude responses at the O1 and M2 frequencies and decreases most hydromechanical parameter estimates by a factor of about 2.5. Failing to include ocean tidal loading leads to an erroneous (perfectly) confined aquifer model.

Plain language summary

The water level in a borehole can respond to pore pressure changes induced in the surrounding aquifer by solid Earth tides, ocean tidal loading at nearby coastlines, and local atmospheric pressure variations. The amplitude and timing of these responses can be used to assess the aquifer's degree of confinement, and to estimate some of the aquifer's hydraulic and mechanical properties. We found that two boreholes established in an ophiolitic, peridotite terrain in the Samail ophiolite (Oman) exhibited markedly different responses to tidal forcing, even though they are separated by a distance of only ~ 100 m, indicating that faults and fractures disrupt the aquifer structure. One of the boreholes (BA1B) does not respond to any tidal forcing, indicating a water table, or unconfined, aquifer. The other borehole (BA1D) responds to both tidal strain and atmospheric pressure in a way that indicates a partially-confined aquifer with low porosity and hydraulic conductivity.

CRediT authorship contribution statement

R.A. Sohn: Software, Formal analysis, Writing – original draft. **J.M. Matter:** Investigation, Resources, Writing – original draft, Project administration, Funding acquisition.

Declaration of Competing Interest

The authors declare that they have no known competing financial interests or personal relationships that could have appeared to influence the work reported in this paper.

Data availability

I have shared the link to my data in the manuscript.

Acknowledgments

The authors gratefully acknowledge constructive reviews by the Associate Editor and an anonymous reviewer. We gratefully acknowledge Todd Rasmussen for reviewing an early version of the manuscript.

Thibaut Barreyre for assistance running tidal prediction software, and support from the Sultanate of Oman Ministry of Regional Municipalities and Water Resources, the Oman Public Authority for Mining, and the Sultan Qaboos University. Drilling and research in the Oman Drilling Project was supported by the Alfred P. Sloan Foundation (in association with the Deep Carbon Observatory, DCO), the International Continental Scientific Drilling Program (ICDP), US National Science Foundation (NSF) Research Grant NSF-EAR-1516300, the Japanese Marine Science and Technology Center (JAMSTEC) and the Japanese Society for the Promotion of Science (JSPS) grant number 16H06347, the US National Aeronautics and Space Administration (NASA, including the Rock Powered Life NASA Astrobiology Institute (NNA15BB02A), the European Science Foundation, the German Science Foundation, the Swiss Science Foundation, and the International Ocean Discovery Program (aka International Ocean Drilling Program, IOPD).

Open research

All of the data and tidal strain estimates used in this paper are available through Zenodo, https://doi.org/10.5281/zenodo.7458164.

References

Agnew, D.C., 1997. NLOADF: A program for computing ocean-tide loading. J. Geophys. Res.: Solid Earth 102 (B3), 5109–5110.

Bastias Espejo, J.M., Rau, G.C., Blum, P., 2022. Groundwater responses to Earth tides: Evaluation of analytical solutions using numerical simulation. J. Geophys. Res.: Solid Earth 127. https://doi.org/10.1029/2022JB024771.

Bower, D.R., 1983. Bedrock Fracture Parameters From the Interpretation of Well Tides. J. Geophys. Res. 88 (B6), 5025–5035.

Bredehoeft, J.D., 1967. Response of well-aquifer systems to Earth tides. J. Geophys. Res. 72 (12), 3075–3087.

Chave, A.D., 2017. Computational Statistics in the Earth Sciences. Cambridge University Press, p. 451 pp.

Christensen, N.I., 1966. Elasticity of Ultrabasic Rocks. J. Geophys. Res. 71 (24), 5921–5931.

Christensen, N.I., 1996. Poisson's ratio and crustal seismology. J. Geophys. Res. 101 (B2), 3139–3156.

Clark, W.E., 1967. Computing the barometric efficiency of a well. J. Hydr. Division 93 (4), 93–98.

Cutillo, P.A., Brehehoeft, J.D., 2011. Estimating aquifer properties from the water level response to Earth tides. Groundwater 49 (4), 600–610. https://doi.org/10.1111/j.1745-6584.2010.00778.x.

Dewandel, B., Lachassagne, P., Boudier, F., Al-Hattali, S., Ladouche, B., Pinault, J.-L., Al-Suleimani, Z., 2005. A conceptual hydrogeological model of ophiolite hard-rock aquifers in Oman based on a multiscale and a multidisciplinary approach. Hydrgeol. J. 13 (5-6), 708–726.

Escartin, J., Hirth, G., Evans, B., 2001. Strength of slightly serpentinized peridotites: Implications for the tectonics of oceanic lithosphere. Geology 29 (11), 1023–1026.

Falcon-Suarez, I., Bayrakci, G., Minshull, T.A., North, L.J., Best, A.I., Roumejon, S., IODP Expeditiion 357 Science Party, 2017. Elastic and electrical properties and permeability of serpentinites from Atlantis Massif, Mid-Atlantic Ridge. Geophys. J. Int. 211, 686–699.

Furbish, D.J., 1991. The response of water level in a well to a time series of atmospheric loading under confined conditions. Water Resour. Res. 27 (4), 557–568.

Fyfe, W.S., 1974. Heats of Chemical Reactions and Submarine Heat Production. Geophys. J. R. Astr. Soc. 37, 213–215. https://doi.org/10.1111/j.1365-246X.1974.tb02454.x.

Hsieh, P.A., Bredehoeft, J.D., Farr, J.M., 1987. Determination of aquifer transmissivity from Earth tide analysis. Water Res. Res. 23 (10), 1824–1832.

Katayama, I., Abe, N., Hatakeyama, K., Akamatsu, Y., Okazaki, K., Ulven, O.I., Hong, G., Zhu, W., Cordonnier, B., Michibayashi, K., Godard, M., Kelemen, P., 2020. Permeability profiles across the crust-mantle sections in the Oman Drilling Project inferred from dry and wet resistivity data. J. Geophys. Res. Solid Earth 125 (8). https://doi.org/10.1029/2019JB018698.

Kelemen, P. B., J. M. Matter, D. A. H. Teagle, J. A. Coggon, and the Oman Drilling Project Science Team (2021a), Proceedings of the Oman Drilling Project: College Station, TYX, https://doi.org/10.14379/OmanDP.proc.2020.

Kelemen, P. B., J. A. Leong, J. C. de Obeso, J. M. Matter, E. T. Ellison, A. Templeton, D. B. Hothaft, A. Eslami, K. Evans, M. Godard, B. Malvoisin, J. A. Coggon, N. H. Warsi, P. Pezard, S. Choe, D. A. H. Teagle, K. Michibayashi, E. Takazawa, Z. Al Sulaimain, and The Oman Drilling Project Science Team (2021b), Initial Results From the Oman Driolling Project Muli-Borehole Observatory: Petrogenesis and Ongoing Alteration of Mantle Peridotite in the Weathering Horizon, *J. Geophys. Res. Solid Earth, 126*, e2021JB022729, https://doi.org/10.1029/2021JB022729.

Kelemen, P.B., Matter, J., Streit, E.E., Rudge, J.F., Curry, W.B., Blusztajn, J., 2011. Rates and Mechanisms of Mineral Carboniation in Peridotite: Natural Processes and Recipes for Enhanced, in situ CO2 Capture and Storage. Annu. Rev. Earth Planet. Sci. 39, 545–576. https://doi.org/10.1146/annurev-earth-092010-152509.

Liang, X., Wang, C.-Y., Ma, E., Zhang, Y.-K., 2022. Effects of unsaturated flow on hydraulic head response to Earth tides – An analytical model. Water Resour. Res. 58 https://doi.org/10.1029/2021WR030337.

Lods, G., Roubinet, D., Matter, J.M., Leprovost, R., Gouze, P., Oman Drilling Project Science Team, 2020. Groundwater flow characterization of an ophiolitic hard-rock aquifer from cross-borehole multi-level hydraulic experiments. J. Hydrology 589. https://doi.org/10.1016/j.hydrol.2020.125152.

Macdonald, A.H., Fyfe, W.S., 1985. Rate of serpentinization in seafloor environments. Tectonophysics 116, 123–135. https://doi.org/10.1016/0040-1951(85)90225-2.

Marechal, J.C., Dewandel, B., Subrahmanyam, K., Torri, R., 2003. Specific methods for the evaluation of hydraulic properties in fractured hard-rock aquifers. Curr. Sci., Indian Acad. Sci. 85 (4), 511–516.

Marechal, J.C., Dewandel, B., Ahmed, S., Galeazzi, L., Zaidi, F.K., 2006. Combined estimation of specific yield and natural recharge in a semi-arid groundwater basin with irrigated agriculture. J. Hydrology 329, 281–293. https://doi.org/10.1016/j.jhydrol.2006.02.022.

McCollom, T.M., Seewald, J.S., 2001. A reassessment of the potential for reduction of dissolved CO2 to hydrocarbons during serpentinization of olivine. Geochim. Cosmo. Acta 65 (21), 3769–3778. https://doi.org/10.1016/S0016-7037(01)00655-X.

McMillan, T.C., Rau, G.C., Timms, W.A., Andersen, M.S., 2019. Utilizing the impact of Earth and Atmospheric tides on groundwater systems: A review reveals the future potential. Rev. Geophys. 57 (2), 281–315.

Nothaft, D.B., Templeton, A.S., Boyd, E.S., Matter, J.M., Stute, M., Paukert Vankeuren, A. N., 2021. Aqueous geochemical and microbial variation across discrete depth intervals in a peridotite aquifer assessed using a packer system in the Samail Ophiolite Oman. JGR Biogeosciences 126 (9). https://doi.org/10.1029/2021JG006319.

Percival, D.B., Walden, A.T. (Eds.), 1993. Spectral Analysis for Physical Applications. Cambridge University Press.

Rasmussen, T.C., Crawford, L.A., 1997. Identifying and removing barometric pressure effects in confined and unconfined aquifers. Ground Water 35 (3), 502–511.

Rau, G.C., 2018. PyGTide: A Python module and wrapper for ETERNA PREDICT to compute synthetic model tides on Earth. Zenodo. https://doi.org/10.5281/zenodo.1346260.

Rau, G.C., Cuthbert, M.O., Acworth, R.I., Blum, P., 2020. Technical note: Disentangling the groundwater response to Earth and atmospheric tides to improve subsurface characterization. Hydrol. Earth Syst. Sci. 24, 6033–6046. https://doi.org/10.5194/hess-24-6033-2020.

Reinen, L.A., Weeks, J.D., Tullis, T.E., 1994. The Frictional Behavior of Lizardite and Antigorite Serpentinites: Experiments, Constitutive Models, and Implications for Natural Faults. Pure Appl. Geophys. 143 (1), 317–358.

Rojstaczer, S., 1988. Determination of fluid flow properties from the response of water levels in wells to atmospheric loading. Water Res. Res. 24 (11), 1927–1938.

Rojstaczer, S., Agnew, D.C., 1989. The influence of formation material properties on the response of water levels in wells to Earth tides and atmospheric loading. J. Geophys. Res. 94 (B9), 12403–12411.

Rojstaczer, S., Riley, F.S., 1990. Response of the water level in a well to Earth tides and atmospheric loading under unconfined conditions. Water Res. Research 26 (8), 1803–1817.

Schrenk, M.O., Brazelton, W.J., Lang, S.Q., 2013. Serpentinization, Carbon, and Deep Life. Rev. Mineral. Geochem. 75, 575–606.

Templeton, A.S., Ellison, E.T., Glombitza, C., Morono, Y., Rempfert, K.R., Hoehler, T.M., Zeigler, S.D., Kraus, E.A., Spear, J.R., Nothaft, D.B., Fones, E.M., Boyd, E.S., Munro-Ehrlich, M., Mayhew, L.E., Cardace, D., Matter, J.M., Kelemen, P.B., the Oman Drilling Project Science Party, 2021. Accessing the subsurface biosphere within rocks undergoing active low-temperature serpentinisation in the Samail Ophiolite (Oman Drilling Project). J. Geophys. Res. Biogeosci. 126.

Ternieten, L., Fruh-Green, G.L., Bernasconi, S.M., 2021. Carbon Geochemistry of the Active Serpentinization Site at the Wadi Tayin Massif: Insights From the ICDP Oman Drilling Project: Phase II. e2021JB022712 J. Geophys. Res. Solid Earth 126. https://doi.org/10.1029/2021JB022712.

Thomson, D.J., 1982. Spectrum estimation and harmonic analysis. Proc. IEEE 70 (9), 1055–1096.

Van der Kamp, G., Gale, J.E., 1983. Theory of Earth tide and barometric effects in porous formations with compressible grains. Water Res. Res. 19 (2), 538–544.

Wang, C.-Y., Doan, M.-L., Xue, L., Barbour, A.J., 2018. Tidal response of groundwater in a leaky aquifer – Application to Oklahoma. Water Resour. Res. 54, 8019–8033. https://doi.org/10.1029/2018WR022793.

Weeks, E.P., 1979. Barometric fluctuations in wells tapping deep unconfined aquifers. Water Res. Res. 15 (5), 1167–1176.

Zhang, J., Liang, X., Wang, C.-Y., 2023. Capillary impact on tidal response of groundwater in unconfined aquifers with finite thickness, anisoptropy, and wellbore storage – An analytical model. Water Resour. Res. 59 e2022WR033578.